Formation of Ligand Clusters on Multimodal Chromatographic Surfaces

Camille L. Bilodeau[†] (bilodc2@rpi.edu), Edmond Y. Lau[‡] (lau12@llnl.gov), David Roush (david_roush@merck.com), Shekhar Garde[†] (gardes@rpi.edu), Steven M. Cramer[†] (crames@rpi.edu)*

[†]Howard P. Isermann Department of Chemical and Biological Engineering and Center for Biotechnology and Interdisciplinary Studies, Rensselaer Polytechnic Institute, 110 Eighth Street, Troy, New York 12180, United States of America

[‡]Physical and Life Sciences Directorate, Lawrence Livermore National Laboratory, Livermore, California, 94550, United States of America

*Biologics and Vaccines, Downstream Process Development and Engineering, Merck & Co., Inc., Kenilworth, NJ, 07033, United States of America

Abstract:

Multimodal chromatography is a powerful tool that uses multiple modes of interaction, such as charge and hydrophobicity, to purify protein-based therapeutics. In this work, we performed molecular dynamics (MD) simulations of a series of multimodal cation exchange ligands immobilized on a hydrophilic self-assembled monolayer (SAM) surface at the commercially relevant surface density (1 ligand/nm^2). We found that ligands that were flexible and terminated

in a hydrophobic group had a propensity to aggregate on the surface, while less flexible ligands containing a hydrophobic group closer to the surface did not aggregate. For aggregating ligands, this resulted in the formation of a surface pattern that contained relatively large patches of hydrophobicity and charge whose sizes exceeded the length scale of the individual ligands. On the other hand, lowering the surface density to 1 ligand/ 3 nm^2 reduced or eliminated this aggregation behavior. In addition, the introduction of a flexible linker (corresponding to the commercially available ligand) enhanced cluster formation and allowed aggregation to occur at lower surface densities. Further, the use of flexible linkers enabled hydrophobic groups to collapse to the surface, reducing their accessibility. Finally, we developed an approach for quantifying differences in the observed surface patterns by calculating distributions of patch size and patch length. This clustering phenomenon is likely to play a key role in governing protein-surface interactions in multimodal chromatography. This new understanding of multimodal surfaces has important implications for developing improved predictive models as well as designing new classes of multimodal separation materials.

1. Introduction

Multimodal (MM) chromatography has recently emerged as a powerful tool for achieving challenging protein separations[1]. Unlike single mode chromatography methods such as ion-exchange chromatography (IEX) or hydrophobic interaction chromatography (HIC), multimodal chromatography separates proteins using ligands that are capable of multiple modes of interaction, including charge, hydrogen bonding, hydrophobic, and aromatic interactions. By leveraging multiple modes of interaction on a single ligand, multimodal resins have been shown to be able to purify difficult-to-separate proteins[2–5]. Despite this, multimodal ligand-protein interactions have

proven to be challenging to understand and predict, limiting the use of multimodal chromatography in industry[1,6].

To address this challenge, our lab has carried out a series of fundamental studies to elucidate multimodal-ligand protein interactions. Cramer and co-workers[4,7–10] have employed NMR in free solution and with ligand-coated nanoparticles as well as molecular dynamics (MD) simulations and AFM experiments to identify and study a preferred binding face for Ubiquitin interacting with two multimodal cation exchange resins, Capto MMC and Nuvia cPrime. In particular, they found that both ligands preferred to interact with a face of Ubiquitin containing proximal regions of charge and hydrophobicity[4,7–10]. In addition, Woo et al. and Robinson et al. used chromatography experiments to characterize the selectivities of many multimodal ligands on a library of model proteins resulting in the identification of heuristic design rules for the effect of ligand structure on selectivity[11–13]. One limitation of these studies was that they predominantly considered protein-ligand interactions as a function of the individual ligand structure. In a chromatographic setting, multimodal ligands are often immobilized at a sufficiently high surface density, such that they can alter one another's conformation and presentation to an adsorbing protein.

Intermolecular interactions between molecules immobilized at high surface densities have been studied for a wide range of systems, including self-assembled monolayers (SAMs), polymer brushes, and high-density peptide coated surfaces. SAMs take advantage of lateral, non-covalent interactions between neighboring immobilized alkyl or aromatic chains to yield a molecularly ordered surface[14–17]. By adjusting the head group chemistry as well as by making perturbations to the chains themselves, such as adjusting their length or composition, researchers have leveraged intermolecular interactions to design surfaces to address a wide range of applications from biosensors to electronics[17].

Polymer brushes represent another system that includes flexible molecules (typically polymers) grafted to surfaces[18]. Polymer brushes exhibit a transition from a "mushroom" (molecules that are sufficiently spaced so as not to interact with one another) to "brush" (closely packed molecules) configuration with decreasing inter-polymer spacing and as a function of polymer radius of gyration[19,20]. Additionally, researchers have studied di-block co-polymers grafted to substrates and characterized complex relationships between polymer structure and block size, flexibility, and solvent affinity[21,22]. In recent years, these grafted co-polymers have been engineered to respond to specific changes in solvent conditions including salt and pH[23–25].

Systems containing multimodal chromatographic ligands importantly differ from SAMs and polymer brush systems in that these ligands are comparatively short and contain regions of charge, hydrophobicity, and hydrogen bonding in proximity to one another. Here, we investigate for the first time the formation of ligand clusters on multimodal chromatographic surfaces using MD simulations. We study the role that ligand chemistry, surface density, and linker length play in governing the location and relative accessibility of different ligand moieties on a multimodal surface. Further, we develop an approach for systematically quantifying pattern formation on multimodal ligand-coated surfaces. This investigation elucidates how previously studied self-assembly phenomena extend to this class of short, flexible, multimodal molecules with important implications for improving our understanding of protein-surface interactions in multimodal chromatography.

2. Methods

2.1 Simulations of One, Two, and Three MM Ligands Immobilized on a SAM Surface

Sets of one, two, and three ligands were immobilized on an alkyl thiol self-assembled monolayer (SAM) surface using the same setup as has been described by our group previously[26,27]. We

summarize this setup here for completeness. Each ligand was immobilized by covalently bonding its base atom (shown in green in **Figure 1**) to an alkyl thiol chain comprising ten carbons with one sulfur and carbon atom at the base as shown in **Figure 2**. The sulfur atom and seventh carbon from the sulfur were both restrained with a harmonic potential of 1,000 kcal/mol*Å^2 to maintain the structure of the surface, as has been done previously[26,28,29]. The position and orientation of the SAM strands were specified based on parameters corresponding to an alkyl thiol SAM immobilized on a gold (1 1 1) surface as described by Love et al[16]. The box size was chosen to ensure periodicity in the *x* and *y* directions. Ligand parameters were consistent with General Amber Force Field (GAFF)[30] and charges were calculated in Gaussian using the Restrained Electrostatic Potential (RESP) approach[31]. These parameters are consistent with our previous simulations of ligands in free solution[32].

The surface was constructed from an array of SAM strands terminating in either ligands or hydroxyl groups (to create a hydrophilic reference background). The hydroxyl-terminated strands were constructed similarly to ligand SAM strands, with OH groups parameterized based on GAFF parameters and RESP charges derived from methanol. This hydroxyl terminated SAM surface is hydrophilic[26] and representative of the agarose or polyacrylamide base matrix found in Capto MMC and Nuvia cPrime resins respectively. For systems containing two or three ligands, ligands were separated by a distance of ~1 nm, corresponding to the expected separation on a chromatographic surface at a typical ligand density. Each simulation contained a total of 80 alkyl thiol strands.

Each simulation was performed using AMBER16[33] in the NVT ensemble. Four simulations of 50 ns were performed with different initial velocities, each saving coordinates every 2 ps. Simulations were performed using the GPU accelerated version of pmemd[34,35]. Electrostatics were

calculated using the Particle-Mesh Ewald[36] method with a grid spacing of 0.1 nm, an order of 4 for the B-spline interpolation, and a direct sum tolerance of 10^{-5} (consistent with default parameters). The nonbonded cutoff was 0.9 nm. The Berendsen[37] thermostat was used to maintain the simulation temperature at 298K and the box size was 4.0 x 4.3 x 6 nm^3. The TIP3P model was used to model water and sodium counterions were used for electroneutrality[38]. The number of sodium ions matched the number of ligands in each simulation. Bonds containing hydrogens were constrained using SHAKE and a time step of 2 fs was used.

2.2 Simulations of MM Ligands Immobilized on a SAM Surface at High and Low Densities

To understand ligand conformational equilibria in commercially available resins, simulations were carried out at both high (1 ligand/nm^2) and low (1 ligand/ 3 nm^2) ligand densities, which correspond to the commercially available densities for Capto MMC and Capto MMC ImpRes, respectively[11]. The low density SAM surfaces were constructed as described in the above section, with the box size expanded to 10.0 x 10.4 x 10.0 nm^3. Each simulation contained 480 alkyl thiol SAM strands with 30 strands terminating in a ligand and the remainder terminating in a hydroxyl group. The high density SAM surfaces were constructed with a slightly larger box size of 11.0 x 10.4 x 10.0 nm^3 in order to ensure that the ligand placement pattern was not affected by the periodic boundary conditions at the edge fo the box. Each simulation contained 528 alkyl thiol SAM strands with 132 strands terminating in a ligand and the remainder terminating in a hydroxyl group. Each setup was simulated 8 times for 50 ns with different initial velocities and the details of the simulation were the same as above.

3. Results

Selectivity in multimodal chromatographic systems has been shown to be a strong function of both ligand structure and point of immobilization[11,12]. Here, we employ molecular dynamics

simulations to study the behavior of multimodal ligands on a model, hydrophilic self-assembled monolayer (SAM) surface representing the resin base-matrix. This investigation focuses on two commonly used, commercially available multimodal ligands: Capto MMC and Nuvia cPrime, shown in **Figures 1a and 1b**. Both ligands contain four chemical groups, of which three are identical: a carboxylic acid group, an amide group, and a phenyl ring. Capto MMC is immobilized to the chromatographic surface via an alkyl thiol group such that the phenyl ring is outward facing (illustrated in **Figure 1a**). In contrast, Nuvia cPrime is immobilized to the chromatographic surface by an amine group, such that the carboxylic acid group is outward facing (**Figure 1b**).

In the commercially available resin, Capto MMC is immobilized via an ester linkage connected to the alkyl thiol group. In the first part of this paper, instead of the ester linkage we immobilize Capto MMC directly to the surface to facilitate direct comparison of the ligand chemistries of Capto MMC and Nuvia cPrime. In the second part, we explore the consequences of including the ester linker (illustrated in **Figure 1c**) and of reducing ligand density. To clarify, when we are not including a linker, we refer to Capto MMC without a linker as the "Capto Ligand" and Capto MMC with the linker as "Capto MMC".

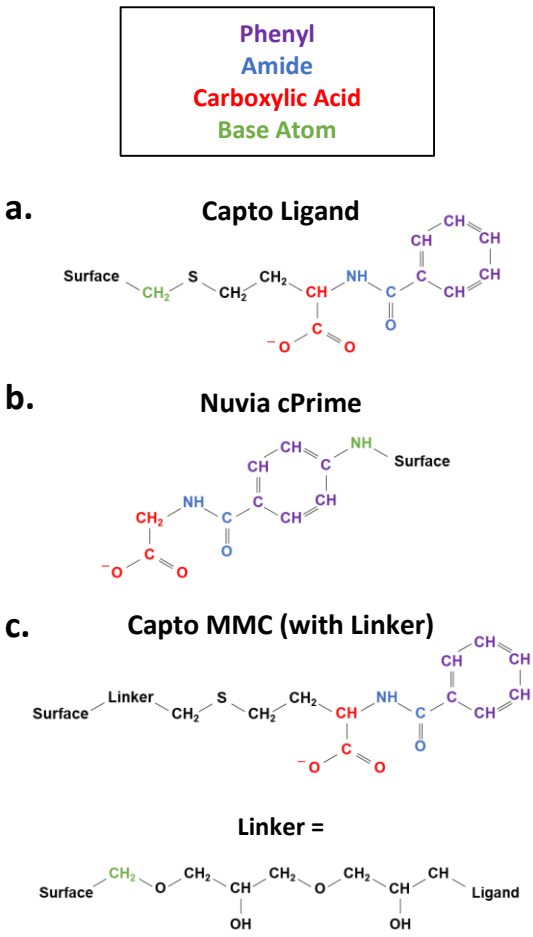

Figure 1. Chemical structures for the **(a)** Capto Ligand (Capto MMC without a linker), **(b)** Nuvia cPrime, and **(c)** Capto MMC (with a linker). Color indicates the type of chemical moiety.

3.1 Capto Ligand and Nuvia cPrime: One, Two, and Three MM Ligands Immobilized on a SAM Surface

Before investigating the behavior of complex higher ligand density systems, it was of interest to first examine the behavior of individual MM ligands immobilized on the SAM surface. The conformational preferences of the Capto Ligand and Nuvia cPrime can be characterized in many ways. Here, we quantified ligand conformational preferences with respect to the surface by calculating the density distributions of two chemical moieties in the ligand, the carboxylic acid group and the phenyl ring, in the *x*-*y* plane of the surface. We characterize conformation with

respect to the surface normal (*z* dimension) later in this manuscript. The first 5ns of each trajectory were used as equilibration time, and thus each density distribution shown represents the last 45ns of four 50ns simulations. An example snapshot of a simulation containing a single Capto Ligand immobilized on a surface is shown in **Figure 2**.

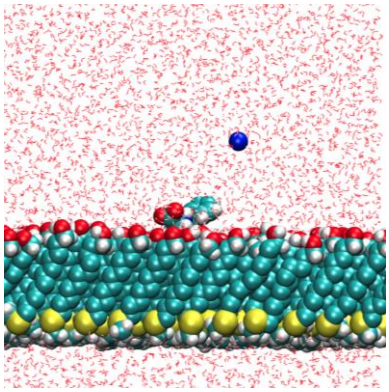

Figure 2. A representative snapshot from MD simulations of a single Capto Ligand immobilized on a hydroxyl SAM surface (spacefill) in water (wireframe) with a sodium counterion (spacefill). The 3D periodic box had dimensions of ~4 x 4 x 4 nm^3. Color scheme: sodium, blue; hydrogen, white; oxygen, red; carbon, cyan; nitrogen, blue; and sulfur, yellow.

Figure 3a shows the probability density distributions for a single Capto Ligand immobilized on the SAM surface. The base atom density (green) illustrates the position at which the ligand is tethered to the SAM surface. As expected, based on the ligand structure (**Figure 1a**), the carboxylic acid density (red) was constrained closer to the base atom and the phenyl ring density (purple) travelled farther from the point of immobilization. Further, the phenyl ring sampled positions in all directions relative to the base atom (although it displayed a preference for one direction due to the method angle of attachment to the tilted SAM surface, breaking symmetry).

Figure 3b shows the probability density distributions for two Capto Ligands immobilized on a SAM surface at a distance corresponding to the average ligand density for the commercial Capto MMC resin. For this system, phenyl ring densities (purple) shift to the region between the two

ligands, indicating that interactions between neighboring ligands significantly impacted ligand conformational preferences. A representative snapshot (shown in **Figure 3b**) clearly shows the association of the phenyl rings, which is likely due to hydrophobic interactions. Similarly, phenyl ring densities were found to increase in the regions between ligands for three Capto Ligands immobilized on a SAM surface (shown in **Figure 3c**). For this system, ligands were found to either completely associate with one another, or to associate in pairs, excluding the third ligand (as shown in the snapshot in **Figure 3c**). In addition, minimal changes were observed in the carboxylic acid density (red) for either the two or three ligand systems.

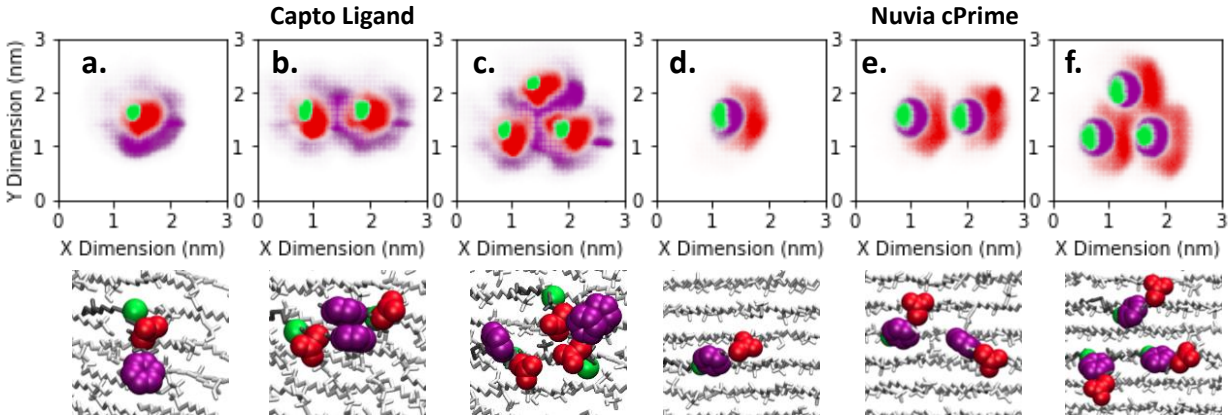

Figure 3. Top: Density distributions in the plane of the surface for the phenyl ring (purple), carboxylic acid group (red), and base atom (green). Results were obtained using four 50ns trajectories (averaged). Bottom: Representative snapshots of ligands where the phenyl ring, carboxylic acid, and base atom are shown in space-fill (same color scheme) and all other atoms are shown in white with licorice representation. **(a)**, **(b)**, and **(c)** correspond to systems containing one, two, and three Capto Ligands immobilized respectively and **(d)**, **(e)**, and **(f)** correspond to systems containing one, two, and three Nuvia cPrime ligands immobilized respectively.

Figure 3d shows the probability density distributions for a single Nuvia cPrime ligand on a SAM surface. In contrast to the Capto Ligand, Nuvia cPrime displayed limited flexibility, with each moiety extending in only one direction from the base atom. There are two effects that could be driving this difference in conformational preferences. First, Nuvia cPrime contains only five

freely rotatable torsion angles (compared to eight in the Capto Ligand) and these torsion angles are located above the phenyl ring and thus farther from the point of immobilization. This constrains the overall flexibility of Nuvia cPrime when immobilized. Second, Nuvia cPrime terminates in a hydrophilic carboxylic acid group, which prefers to remain solvated rather than collapse to the surface. In contrast, the Capto Ligand terminates in a hydrophobic phenyl ring, which has a propensity to desolvate and to associate with the SAM surface as will be shown later in this manuscript. These structural differences between Nuvia cPrime and the Capto Ligand result in significantly different conformational preferences when immobilized on a surface.

Figure 3e shows the probability density distributions for two Nuvia cPrime ligands immobilized on a SAM surface at a distance corresponding to that of a standard chromatography resin. In contrast to the Capto Ligand, neighboring Nuvia cPrime ligands did not interact with one another, but rather maintained approximately the same density distributions as were observed for the single ligand case (**Figure 3d**). This effect is further illustrated in the representative snapshot shown in **Figure 3e**, which shows two neighboring ligands that are not contacting one another. This lack of interaction is consistent with 1) the inherent lack of flexibility resulting from the Nuvia cPrime structure and 2) electrostatic repulsion between carboxylic acid groups on neighboring ligands. For three Nuvia cPrime ligands immobilized on a SAM surface (**Figure 3f**), we again found that ligand conformational preferences were not affected by neighboring ligands.

3.2 Ligands Immobilized at a Constant Ligand Density on a SAM Surface

In a chromatography resin, ligands do not interact with just one or two neighboring ligands but have the potential to interact with a large number of neighboring ligands on a continuously ligand-coated surface. Thus, it was of interest to understand how ligand conformational preferences changed in this more complex scenario. **Figure 4a** shows the density distributions associated with

the Capto Ligand immobilized continuously at the ligand density associated with the Capto MMC resin (1 ligand/1 nm^2). As was observed for sets of 2-3 ligands, interactions were again observed between the phenyl rings of neighboring ligands (shown in **Figure 4b**). Importantly, for this more complex system, this resulted in the formation of large phenyl ring clusters (purple) containing roughly 3-4 phenyl rings that stayed together throughout the length of the simulation. Further, the carboxylic acid groups (red) were found to move closer to one another (although they did not form direct contacts), pulled by the phenyl rings which interact with each other. Thus, ligand-ligand interactions caused the aggregation of ligands leading to a complex, multimodal surface containing highly hydrophobic patches (purple) and regions of concentrated charge (red) that were on length scales larger than any individual ligand. We believe that the relative length-scales of these patches may play an important role in governing protein-resin interactions and selectivity in these systems. This principle is discussed in greater detail later in this manuscript.

Figure 4c shows the density distributions associated with Nuvia cPrime immobilized at the same ligand density. As was observed in the previous section for one, two, and three Nuvia cPrime ligands, neighboring ligands at this continuous ligand density remained separate. This resulted in conformational preferences for each individual ligand that were similar to those of the single ligand alone on a hydroxyl SAM surface. This lack of interaction between neighboring ligands on the Nuvia cPrime surface is in sharp contrast to the results described above for the Capto Ligand and resulted in a multimodal surface that contained hydrophobic and charge patches on a fundamentally smaller length scale.

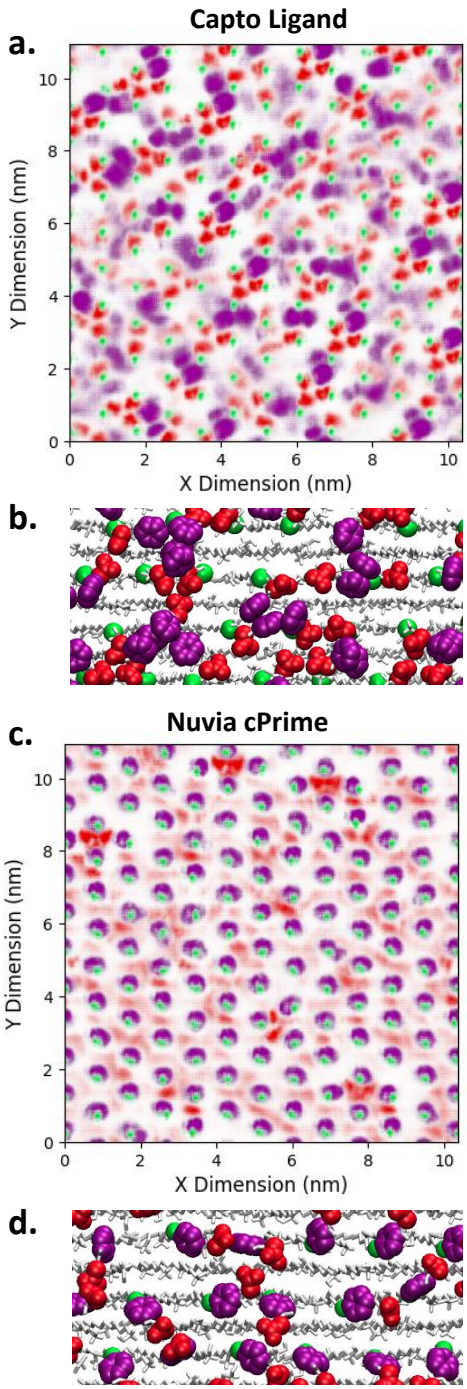

Figure 4. (a)/(c) Density distributions for the Capto Ligand and Nuvia cPrime, respectively, immobilized on a SAM surface at the ligand density associated with the Capto MMC resin. Results were obtained using a single 50ns trajectory. Atom density scale ranges from 0 (white) to 2 atoms/nm^2 (relevant color).**(b)/(d)** Representative snapshots of Capto Ligand and Nuvia cPrime, respectively. Colors: Purple, phenyl ring; red, carboxylic acid group; green, base

atom. Ligand atoms are shown in space-fill (same color scheme) and all other atoms are shown in white with licorice representation.

3.3 Capto Ligand Immobilized at a Low Ligand Density on a SAM Surface

In multimodal chromatography, resins are often available at multiple ligand densities. It was therefore of interest to investigate the role of ligand density on the previously described aggregation phenomenon. Accordingly, simulations of the Capto Ligand were carried out at a lower ligand density (1 ligand/3 nm^2) corresponding to the Capto MMC ImpRes resin. The individual ligand density distributions, shown in **Figure 5a**, were found to resemble that of a single ligand on a surface (**Figure 3a**). At this ligand density, ligands were separated by large enough spacings that they were no longer able to interact strongly. This illustrates that by reducing the ligand density, it is possible to eliminate the ligand aggregation observed at higher ligand densities. Importantly, this illustrates that for ligands that aggregate with one another, increasing or decreasing the ligand density does not simply adjust the apparent affinity through an avidity effect, but can also change the fundamental nature of the resin surface presented to the protein.

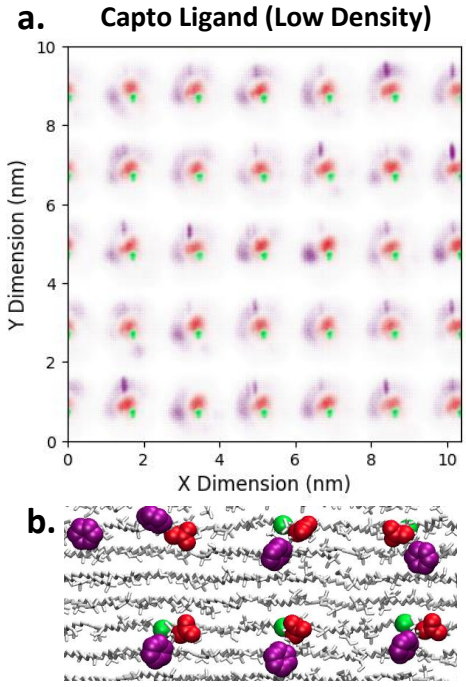

Figure 5. (a) Density distributions for the Capto Ligand immobilized on a SAM surface at the ligand density associated with the Capto MMC ImpRes resin for a single, 50ns trajectory. Results were obtained using a single 50ns trajectory. Atom density scale ranges from 0 (white) to 2 atoms/nm^2 (relevant color). **(b)** Representative snapshot of Capto Ligand. Colors: Purple, phenyl ring; red, carboxylic acid group; green, base atom. Ligand atoms are shown in space-fill (same color scheme) and all other atoms are shown in white with licorice representation.

3.4 Capto MMC (Capto Ligand with a Linker) Immobilized on a SAM Surface

In the previous sections, we studied the conformational preferences of the Capto MMC resin without the linker (referred to here as the Capto Ligand). While excluding the linker provides a simpler system to study that can be more easily compared with the Nuvia cPrime (which does not contain a linker in commercial resin), the ligand in the commercial Capto MMC resin is immobilized to the base matrix via an ester linker (**Figure 1c**). Accordingly, it was of interest to explore the effect of this linker on the conformational preferences of Capto MMC.

Figure 6a shows the density distributions for a Capto MMC (with linker) coated surface at the ligand density associated with the commercial Capto MMC resin (1 ligand/1 nm^2). Although this surface displayed large regions of concentrated phenyl ring densities indicating ligand aggregation, these were accompanied by regions of diffuse phenyl ring densities. As illustrated in **Figure 6b**, regions containing ligand aggregates often included a larger number of ligands than were typically observed for the Capto ligand surface. These differences in conformational preferences were likely due to the fact that the linker enables additional ligand flexibility increasing the region on the surface accessible to the ligand. Further, this additional flexibility results in reduced ordering on the resin surface and allows for a greater number of ligands to interact with one another.

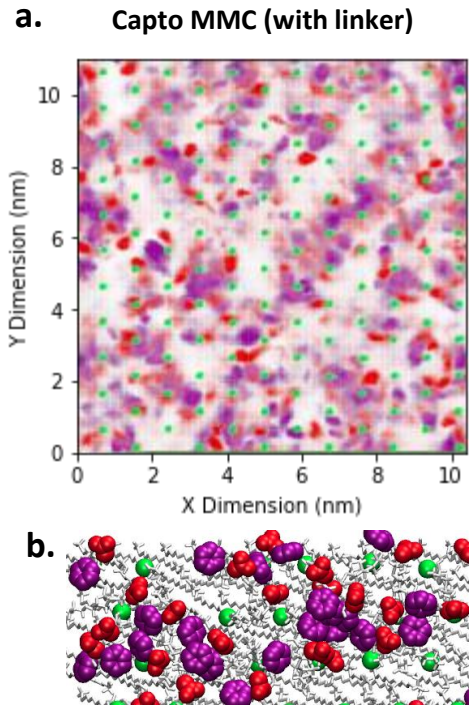

Figure 6. (a) Density distributions for Capto MMC (with the ester linker) immobilized on a SAM surface at the ligand density associated with the Capto MMC resin. Results were obtained using a single 50ns trajectory. Atom density scale ranges from 0 (white) to 2 atoms/nm^2 (relevant color). **(b)** Representative snapshot of Capto MMC. Colors: Purple, phenyl ring; red, carboxylic acid group; green, base atom. Ligand atoms are shown in space-fill (same color scheme) and all other atoms are shown in white with licorice representation.

Figure 7a shows the density distributions for Capto MMC immobilized at the ligand density associated with the commercial Capto MMC ImpRes resin (1 ligand/3 nm^2). In contrast to the Capto Ligand (without the linker) at this lower ligand density, ligands with the linker were found to aggregate with one another, albeit to a lesser extent than the higher density system. This aggregation is expected as the length and flexibility in the linker allows neighboring ligands to travel farther to interact with one another. This observation points to the existence of a critical ligand-ligand separation beyond which ligands can no longer aggregate with one another. By introducing a linker to Capto MMC, we effectively increased this critical ligand-ligand separation

distance. Thus, we expect that it would be possible to eliminate ligand aggregation by further reducing ligand density. We believe that this is an important observation in that ligand aggregation on chromatographic surfaces is a function of the ligand chemistry and architecture, the linker chemistry and flexibility and the ligand density.

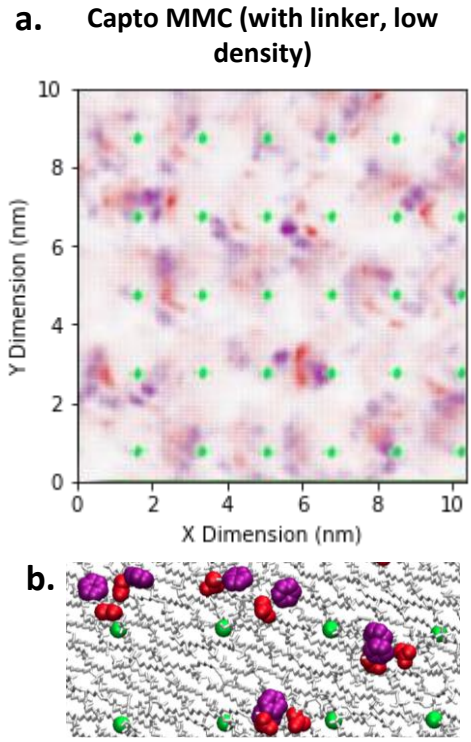

Figure 7. (a) Density distributions for Capto MMC (with the ester linker) immobilized on a SAM surface at the ligand density associated with the Capto MMC ImpRes resin. Results were obtained using a single 50ns trajectory. Atom density scale ranges from 0 (white) to 2 atoms/nm^2 (relevant color). **(b)** Representativef snapshot of Capto MMC. Colors: Purple, phenyl ring; red, carboxylic acid group; green, base atom. Ligand atoms are shown in space-fill (same color scheme) and all other atoms are shown in white with licorice representation.

3.5 Ligand Density Normal to the SAM Surface

When proteins adsorb to chromatographic surfaces, their ability to interact with different ligand chemistries depends, in part, on the steric accessibility of the ligand. To assess the relative

accessibility of different ligand chemistries, we investigated the density distributions of individual chemical moieties along the direction normal to the SAM surface.

Figure 8a shows the heavy atom density distributions for the Capto Ligand phenyl rings (purple) and carboxylic acid groups (red), with the grey vertical dotted line indicating the intersection of the hydroxyl SAM strand density and the solvent density. As shown in **Figure 1a**, the Capto Ligand structure contains the carboxylic acid moiety closer to the point of immobilization and the phenyl ring farther from the point of immobilization. As a consequence of this structure, the carboxylic acid density (red) in **Figure 8a** was distributed close to the surface-water interface. Interestingly, the density distribution for the phenyl ring contained two peaks, one at roughly the same location as the carboxylic acid group and one farther from the surface. This first peak indicates that the phenyl ring did not stretch out into solution, but rather preferred to collapse onto the SAM surface, likely due to its hydrophobicity. The second peak indicated the presence of phenyl rings further from the surface. A representative snapshot from the simulation is presented in **Figure 8b** which illustrates the buried carboxylic acid groups as well as the two populations of phenyl groups.

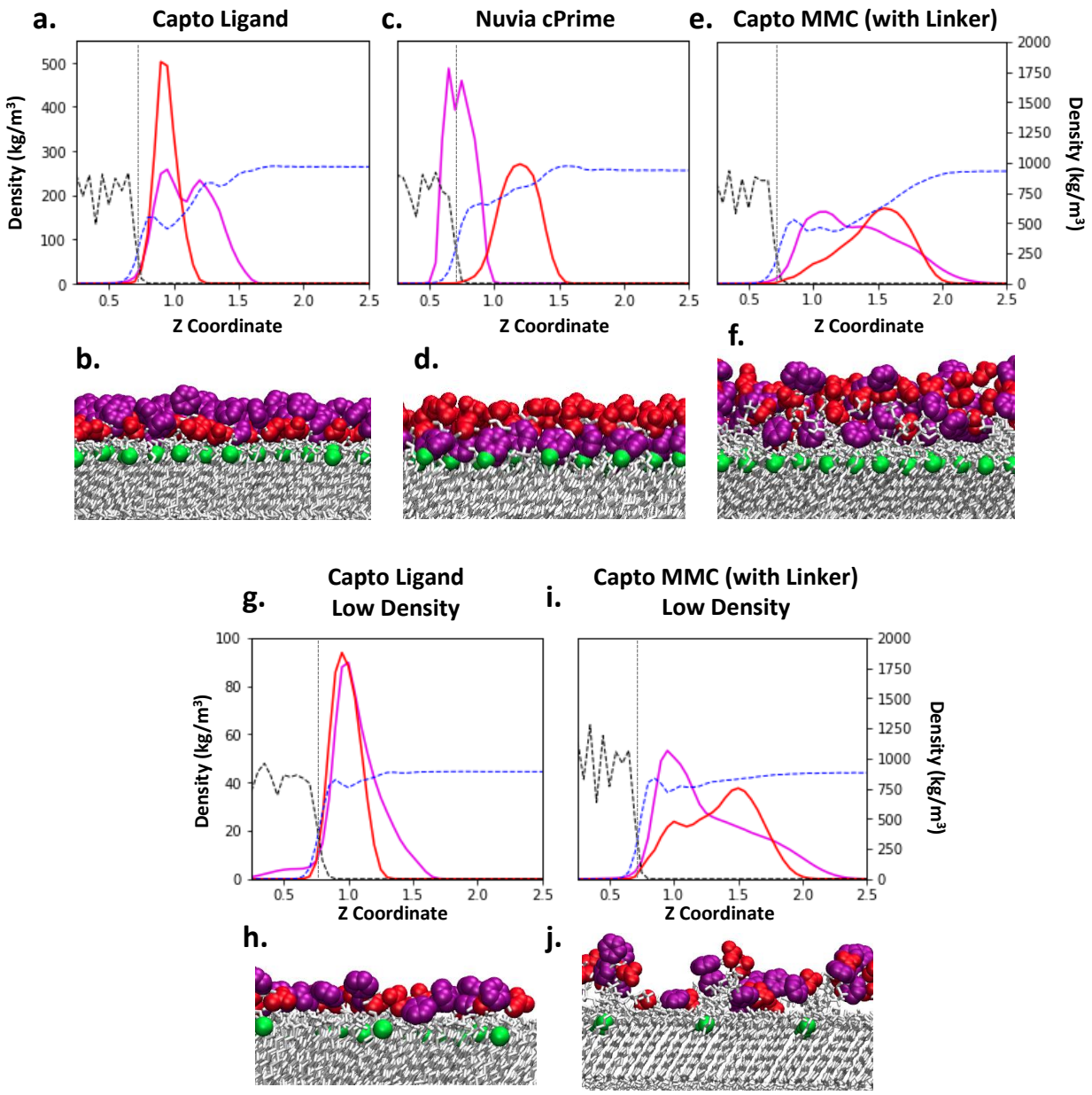

Figure 8. (a), **(c)**, **(e)**, **(g)**, **(i)** Density distributions for the phenyl ring (purple) and carboxylic acid group (red) using the left axis and the hydroxyl SAM surface (dotted black) and water (dotted blue) using the right axis, with the interface between the surface and the solvent marked as a grey dotted line. **(b)**, **(d)**, **(f)**, **(h)**, **(j)** Representative snapshots showing the SAM surface from a side view (same color scheme as Figures 3-7.

Figure 8c shows the density distributions for the Nuvia cPrime phenyl rings (purple) and carboxylic acid groups (red). As shown in **Figure 1b**, Nuvia cPrime contains a phenyl ring linked

to the SAM surface via an amine group as well as a carboxylic acid group farther from the surface. As a consequence of Nuvia cPrime's structure, **Figure 8c** shows that the phenyl ring density overlapped with the solvent-surface interface while the carboxylic acid density was located farther from the surface. Unlike the Capto Ligand, the density distributions of the phenyl rings and the carboxylic acid moieties did not significantly overlap, illustrating that Nuvia cPrime preferred to collapse to the SAM surface. This behavior is further illustrated in **Figure 8d**, which shows a top carboxylic acid layer (red), and buried phenyl rings (purple).

Figure 8e shows the density distributions for Capto MMC (with linker). The inclusion of a flexible linker increased the space sampled by the ligands, resulting in much broader density distributions along the surface normal. Interestingly, the density distribution of the phenyl rings shifted slightly closer to the surface relative to the density distribution of the carboxylic acid groups. A representative snapshot from the simulation is presented in **Figure 8f** which illustrates the broad distribution of the axial positions of both the carboxylic acid groups and the phenyl rings. This behavior was in sharp contrast to the Capto Ligand surface, for which phenyl rings were primarily exposed to the solvent. This difference in behavior can be attributed to the inclusion of the flexible linker which allowed the phenyl rings on the Capto MMC ligand to readily collapse back to the surface. This illustrates that linker length and flexibility can play an important role in governing the degree of accessibility of hydrophobic groups on multimodal ligands which introduces an important element into ligand design.

Figure 8g shows the density distributions for the Capto Ligand at a low ligand density corresponding to that of the commercial Capto MMC ImpRes resin (1 ligand/ 3 nm^2). At this lower ligand density, the carboxylic acid group and phenyl ring density distributions significantly overlapped, and the second phenyl ring peak disappeared. The overlap of these two peaks indicates

that the Capto Ligand at low density was readily able to collapse to the surface rather than extend into solution. In the previous section, we found that ligands at this density were separated by a large enough distance that they could not significantly interact with one another. As a result, the second peak observed in **Figure 8a** at the higher ligand density disappeared at this lower ligand density, suggesting that it results from interactions with neighboring ligands. Additionally, phenyl ring density was observed to penetrate slightly into the SAM surface.

Figure 8i shows the density distributions for Capto MMC (with linker) at a lower ligand density corresponding to that of the Capto MMC ImpRes resin (1 ligand/ 3 nm^2). As was observed for the Capto MMC resin at the higher ligand density, the phenyl ring and carboxylic acid group density distributions were broad, indicating that a range of behaviors could be observed on the surface. Also similar to the high ligand density system, the average phenyl ring density shifted closer to the surface relative to the carboxylic acid group, due to the phenyl ring's preference for collapsing to the surface. As was observed for the lower ligand density without the linker, the ligands have sufficient room to stretch out along the surface as well as to aggregate with one another. This resulted in a highly heterogeneous surface, whose height varied as a function of position on the surface, shown in **Figure 8j**.

3.6 Quantifying Pattern Formation on a Ligand-Covered SAM Surface

In the previous sections, we have investigated ligand aggregation and the formation of patterns of different ligand chemistries on a variety of multimodal SAM surfaces. To systematically study large numbers of resin systems and to create models that capture these surface patches, it is necessary to quantify these patterns. To this end, we have developed an approach for quantifying the size and shape of patches of specific moieties on the ligands.

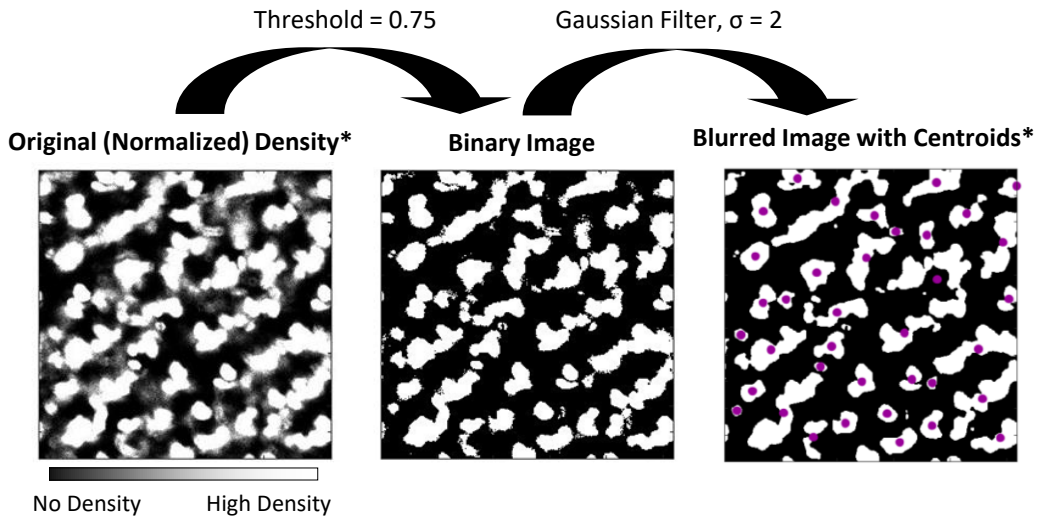

Figure 9. Schematic illustrating approach for obtaining patch distributions for a given ligand chemistry.

Figure 9 illustrates this approach. First, the density distribution was normalized by dividing the density at each point by the average density of the species throughout the surface. This distribution was then converted to a binary distribution based on a cutoff threshold of 0.75. Thus, every grid point in the plane of the surface was assigned a value of 1 if the normalized density exceeded 0.75 or a value of 0 if the normalized density was less than 0.75. This binary distribution was then filtered using a Gaussian filter with a standard deviation of 2 to remove noise around the edges of patches. Finally, using the MATLAB image toolbox, each patch was identified, assigned a centroid, and patch statistics (area, major axis, and minor axis) were calculated. To avoid analyzing noise, patches with an area of less than 0.08 nm^2 (corresponding to ~30% the size of an isolated phenyl ring) were not considered for this analysis. The parameters employed in this approach for quantifying patch distributions were selected to enable good representation of the clusters in the SAM surfaces evaluated. In future work, we will more systematically develop the criteria for determining the relevant parameters in this analysis.

Figure 10a shows analysis using this approach when applied to the phenyl rings on the Capto Ligand surface. The far-left graph shows the binary density distribution for the phenyl rings, with

patch centroids labelled. The resulting area distribution, shown in the center-left graph, illustrates that the average patch size was about 1 nm^2 in size, with some patches reaching areas as large as ~6 nm^2. The major and minor axes (the two right figures) show that these patches were often elongated and could reach major axis lengths of more than 5 nm.

The tendency of the Capto Ligand surface to form large phenyl ring patches has important implications for selectivity in chromatographic systems. In **Figure 10b** and **10c**, we illustrate two, previously studied proteins, ubiquitin and a Fab, with a scale bar. Previous work in our group using NMR, AFM and MD simulations has identified a preferred binding region on the face of ubiquitin for interactions with multimodal ligands and SAM surfaces[4,7–10]. **Figure 10c** illustrates that this face is only roughly 1-2 nm^2 in size and thus the binding region previously identified is likely to interact with only 1-2 phenyl ring patches upon binding to the ligand surface. Additional prior work in our group has suggested that the CDR loops (located at the top of the Fab) play an important role in governing Fab retention in multimodal chromatographic systems[39,40]. **Figure 10c** shows that this region is roughly 4-5 nm in length, suggesting that this protein may only interact with 1-3 phenyl ring patches upon binding to the surface. This analysis suggests that proteins that differ in their patch sizes and/or distributions may interact differently with these large ligand patches, resulting in potentially distinct or advantageous selectivities.

Another important aspect to consider is that these large phenyl ring patches are likely to be more hydrophobic than smaller phenyl ring patches. Previous work in the Garde group[41,42] has shown that the hydrophobicity of hydrophobic patches on a hydrophilic surface undergoes a transition around roughly 1 nm^2, such that small hydrophobic patches below this threshold do not significantly affect local water structure, while larger patches dramatically increase local water density fluctuations. Thus, the association of neighboring phenyl rings on the Capto Ligand SAM

surface results in the crossing of this critical threshold, and likely results in a significantly more hydrophobic surface.

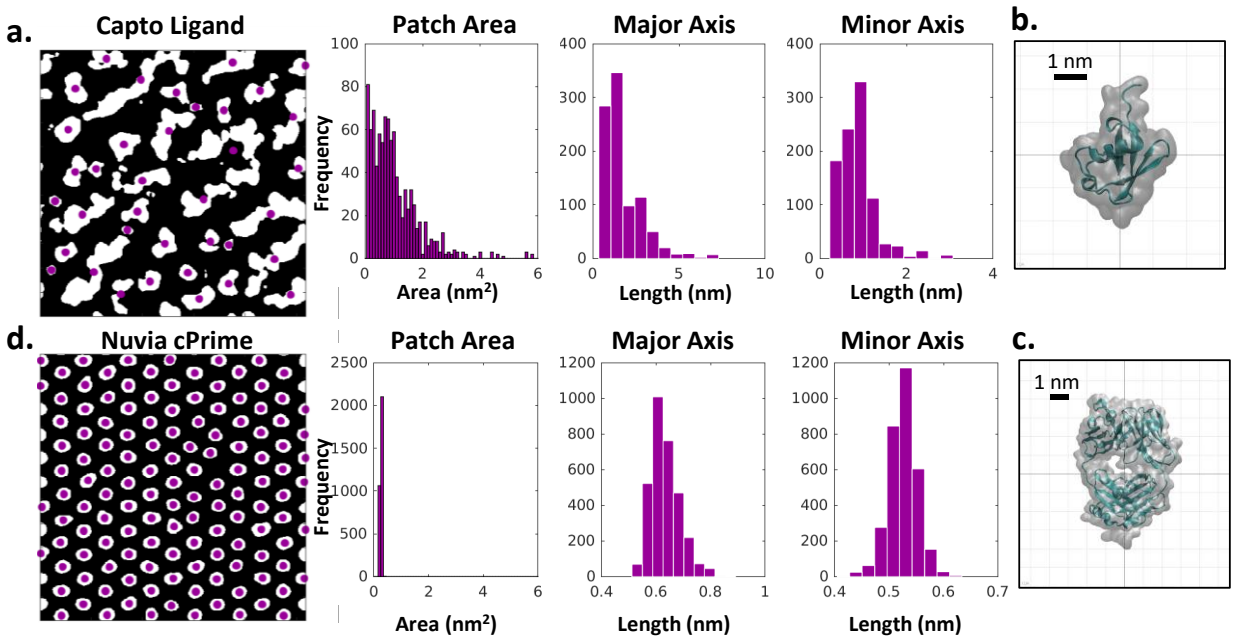

Figure 10. (a), **(d)** Patch statistics for the Capto Ligand. Far-left: Representative filtered, binary, phenyl ring density distribution from a single 50ns simulation with centroids labelled in purple. Center-left: Distribution of patch areas. Center-right: Distribution of patch major axes. Far-right: Distribution of patch minor axes. **(b)**, **(c)** Ubiquitin and an example of a Fab fragment shown as a transparent surface with a ribbon structure underneath. Length scales of 1 nm are shown in the corner to illustrate the length scale of the protein.

Figure 10d shows this approach applied to phenyl ring density for Nuvia cPrime. As was observed in **Figure 4c**, Nuvia cPrime's phenyl rings did not associate with one another, but rather remained separate. As a result, the patch areas were much smaller than those observed for the Capto Ligand, and the distribution was highly mono-dispersed about 0.25 nm^2, with each patch representing one phenyl ring. Similarly, the major and minor axis distributions were relatively monodispersed around much smaller values, varying primarily due to the orientations of the phenyl rings. The differences in shapes and lengthscales of hydrophobic patches on Capto and Nuvia

ligands – large vs small, broad vs monodispersed – will impact the behavior of vicinal water and govern the mechanistic details as well as the strength of protein interactions with the surfaces. Such differences will be important to selectivity despite the chemistries of the two ligands being similar to each other. As described above, we expect that this reduction in the length scale of the hydrophobic patches on the Nuvia cPrime surface affect how many different patches a protein contacts as it adsorbs to the surface and will affect the local water structure in the vicinity of the hydrophobic patches, resulting in a reduction in the strength of hydrophobic interactions.

4. Conclusions

We have performed extensive MD simulations to investigate the formation of ligand clusters on a SAM surface for ligands varying in chemistry, surface density, and linker length. Interestingly, the Capto Ligand was found to aggregate to form a multimodal pattern on the SAM surface, while Nuvia cPrime did not aggregate. Lowering the surface density of the Capto Ligand eliminated clustering, while introduction of a flexible, hydrophilic linker enhanced aggregation and allowed clusters to form at lower surface densities. Finally, we developed an approach to quantify pattern formation on multimodal surfaces and found that the Capto Ligand surface contained patches as large as 6 nm^2, while the Nuvia cPrime surface patches were only ~0.25 nm^2. This work represents the first in depth look at multimodal chromatographic ligand patch formation in the context of a surface.

A comparison of the ligand structures shows that while the Capto Ligand has a hydrophilic group near its base and a hydrophobic group at its terminus, Nuvia cPrime contains the reverse: a hydrophobic group near its base and a hydrophilic group at its end. As a consequence, the hydrophobic phenyl rings on the Capto MMC ligands tended to aggregate and form hydrophobic clusters, while the Nuvia cPrime phenyl rings did not have the flexibility to do so. This

phenomenon is related to the self-assembly behavior previously observed for grafted diblock co-polymers with differing solvent affinities. Zhulina et al[21]. showed that tethering the less soluble block closer to the surface and the more soluble block farther from the surface resulted in the formation of an "onion"-like dense core phase near the surface. In contrast, the opposite arrangement caused the outward facing insoluble block to aggregate resulting in micelle-like structures. The Capto Ligand and Nuvia cPrime can be thought of as a special case of this behavior where each "block" is much smaller and more position restrained than in a traditional block co-polymer. Thus, instead of forming distinct, 3-dimensional phases, we observed the formation of a relatively shallow surface pattern.

In addition, we showed that by reducing the surface density of the Capto Ligand, ligand aggregation was eliminated. In this system, the ligand-ligand spacing was lowered below the Capto Ligand's length, preventing the ligand from interacting with its neighbors. In contrast, Capto MMC (with the linker) represented a system with an increased length, and thus increased accessibility to a larger volume on the surface. Consequently, at the same lowered surface density, Capto MMC's length now exceeded the ligand-ligand spacing, allowing for it to form clusters. This relationship between the ligand-ligand spacing and the length is analogous to the mushroom to brush transition associated with reducing inter-ligand spacing below the radius of gyration of the ligand described by de Genne et al[19]. For the case of multimodal ligand coated surfaces, since there are additional sources of ligand-ligand interactions, this transition may occur at a larger spacing than for polymers interacting only through excluded volume.

Previous work in our group[8,39,40,43] has illustrated that understanding the behavior of patches on the protein surface is important for understanding and predicting chromatographic behavior of proteins in multimodal systems. Here, we show for the first time that hydrophobic and charge

patches exist on not just the protein surface, but also the multimodal ligand surface and it is anticipated that the nature of these surface patterns will have important implications for selectivity in multimodal chromatography. In the future, we aim to apply these characterization approaches to larger libraries of ligands to develop a fundamental understanding of the relationship between individual ligand structure and pattern formation in the context of a surface. Further, we plan to extend these methods to create new classes of molecular descriptors for multimodal surfaces and to employ these descriptors for the development of improved QSPR models for the *a-priori* predict of protein elution and selectivity patterns in novel multimodal resin systems.

Supporting Information. Moiety density distributions for every ligand setup for 5 ns sections during a single simulation and averaged over 45 ns for three different simulations.

5. Acknowledgements

This material is based upon work partially supported by the National Science Foundation under Grant No. (CBET 1704745) as well as the ASC Graduate Fellowship Program from LLNL. The authors would also like to acknowledge helpful discussions with Dr. Mark Snyder from Bio-Rad. Work at the Lawrence Livermore National Laboratory (LLNL) was performed under the auspices of the U.S. Department of Energy by Lawrence Livermore National Laboratory under Contract DE-AC52-07NA27344.

6. References

(1) Cramer, S. M.; Holstein, M. A. Downstream Bioprocessing: Recent Advances and Future Promise. *Current Opinion in Chemical Engineering* **2011**, *1* (1), 27–37. https://doi.org/10.1016/j.coche.2011.08.008.

(2) Shukla, A. A.; Hubbard, B.; Tressel, T.; Guhan, S.; Low, D. Downstream Processing of Monoclonal Antibodies—Application of Platform Approaches. *Journal of Chromatography B* **2007**, *848* (1), 28–39. https://doi.org/10.1016/j.jchromb.2006.09.026.

(3) Kaleas, K. A.; Schmelzer, C. H.; Pizarro, S. A. Industrial Case Study: Evaluation of a Mixed-Mode Resin for Selective Capture of a Human Growth Factor Recombinantly Expressed in E. Coli. *Journal of Chromatography A* **2010**, *1217* (2), 235–242. https://doi.org/10.1016/j.chroma.2009.07.023.
(4) Chung, W. K.; Hou, Y.; Holstein, M.; Freed, A.; Makhatadze, G. I.; Cramer, S. M. Investigation of Protein Binding Affinity in Multimodal Chromatographic Systems Using a Homologous Protein Library. *Journal of Chromatography A* **2010**, *1217* (2), 191–198. https://doi.org/10.1016/j.chroma.2009.08.005.
(5) Gagnon, P.; Cheung, C.; Lepin, E. J.; Wu, A. M.; Sherman, M.; Raubitschek, A. A.; Yazaki, P. J. Minibodies and Multimodal Chromatography Methods: A Convergence of Challenge and Opportunity. *BioProcess international* **2010**, *8* (2), 26–35.
(6) Zhang, L.; Zhao, G.; Sun, Y. Molecular Insight into Protein Conformational Transition in Hydrophobic Charge Induction Chromatography: A Molecular Dynamics Simulation. *The Journal of Physical Chemistry B* **2009**, *113* (19), 6873–6880. https://doi.org/10.1021/jp809754k.
(7) Holstein, M. A.; Chung, W. K.; Parimal, S.; Freed, A. S.; Barquera, B.; McCallum, S. A.; Cramer, S. M. Probing Multimodal Ligand Binding Regions on Ubiquitin Using Nuclear Magnetic Resonance, Chromatography, and Molecular Dynamics Simulations. *Journal of Chromatography A* **2012**, *1229*, 113–120. https://doi.org/10.1016/j.chroma.2011.12.101.
(8) Parimal, S.; Cramer, S. M.; Garde, S. Application of a Spherical Harmonics Expansion Approach for Calculating Ligand Density Distributions around Proteins. *The Journal of Physical Chemistry B* **2014**, *118* (46), 13066–13076. https://doi.org/10.1021/jp506849k.
(9) Srinivasan, K.; Parimal, S.; Lopez, M. M.; McCallum, S. A.; Cramer, S. M. Investigation into the Molecular and Thermodynamic Basis of Protein Interactions in Multimodal Chromatography Using Functionalized Nanoparticles. *Langmuir* **2014**, *30* (44), 13205–13216. https://doi.org/10.1021/la502141q.
(10) Srinivasan, K.; Banerjee, S.; Parimal, S.; Sejergaard, L.; Berkovich, R.; Barquera, B.; Garde, S.; Cramer, S. M. Single Molecule Force Spectroscopy and Molecular Dynamics Simulations as a Combined Platform for Probing Protein Face-Specific Binding. *Langmuir* **2017**, *33* (41), 10851–10860. https://doi.org/10.1021/acs.langmuir.7b03011.
(11) Woo, J.; Parimal, S.; Brown, M. R.; Heden, R.; Cramer, S. M. The Effect of Geometrical Presentation of Multimodal Cation-Exchange Ligands on Selective Recognition of Hydrophobic Regions on Protein Surfaces. *Journal of Chromatography A* **2015**, *1412*, 33–42. https://doi.org/10.1016/j.chroma.2015.07.072.
(12) Woo, J. A.; Chen, H.; Snyder, M. A.; Chai, Y.; Frost, R. G.; Cramer, S. M. Defining the Property Space for Chromatographic Ligands from a Homologous Series of Mixed-Mode Ligands. *Journal of Chromatography A* **2015**, *1407*, 58–68. https://doi.org/10.1016/j.chroma.2015.06.017.
(13) Robinson, J.; Snyder, M. A.; Belisle, C.; Liao, J.; Chen, H.; He, X.; Xu, Y.; Cramer, S. M. Investigating the Impact of Aromatic Ring Substitutions on Selectivity for a Multimodal Anion Exchange Prototype Library. *Journal of Chromatography A* **2018**, *1569*, 101–109. https://doi.org/10.1016/j.chroma.2018.07.049.
(14) Schreiber, F.; Eberhardt, A.; Leung, T. Y. B.; Schwartz, P.; Wetterer, S. M.; Lavrich, D. J.; Berman, L.; Fenter, P.; Eisenberger, P.; Scoles, G. Adsorption Mechanisms, Structures, and Growth Regimes of an Archetypal Self-Assembling System: Decanethiol on Au(111). *Phys. Rev. B* **1998**, *57* (19), 12476–12481. https://doi.org/10.1103/PhysRevB.57.12476.

(15) Castner, D. G.; Ratner, B. D. Biomedical Surface Science: Foundations to Frontiers. *Surface Science* **2002**, *500* (1–3), 28–60. https://doi.org/10.1016/S0039-6028(01)01587-4.
(16) Love, J. C.; Estroff, L. A.; Kriebel, J. K.; Nuzzo, R. G.; Whitesides, G. M. Self-Assembled Monolayers of Thiolates on Metals as a Form of Nanotechnology. *Chemical Reviews* **2005**, *105* (4), 1103–1170. https://doi.org/10.1021/cr0300789.
(17) Casalini, S.; Bortolotti, C. A.; Leonardi, F.; Biscarini, F. Self-Assembled Monolayers in Organic Electronics. *Chem. Soc. Rev.* **2017**, *46* (1), 40–71. https://doi.org/10.1039/C6CS00509H.
(18) Zhao, B.; Brittain, W. J. Polymer Brushes: Surface-Immobilized Macromolecules. *Progress in Polymer Science* **2000**, *25* (5), 677–710. https://doi.org/10.1016/S0079-6700(00)00012-5.
(19) de Gennes, P. G. Conformations of Polymers Attached to an Interface. *Macromolecules* **1980**, *13* (5), 1069–1075. https://doi.org/10.1021/ma60077a009.
(20) Singh, N.; Cui, X.; Boland, T.; Husson, S. The Role of Independently Variable Grafting Density and Layer Thickness of Polymer Nanolayers on Peptide Adsorption and Cell Adhesion. *Biomaterials* **2007**, *28* (5), 763–771. https://doi.org/10.1016/j.biomaterials.2006.09.036.
(21) Zhulina, E. B.; Singh, C.; Balazs, A. C. Self-Assembly of Tethered Diblocks in Selective Solvents. *Macromolecules* **1996**, *29* (25), 8254–8259. https://doi.org/10.1021/ma9606420.
(22) Wang, Z.; Li, B.-H. Self-Assembly of Block Copolymers Grafted onto a Flat Substrate: Recent Progress in Theory and Simulations. *Chinese Phys. B* **2016**, *25* (1), 016402. https://doi.org/10.1088/1674-1056/25/1/016402.
(23) Nath, N.; Chilkoti, A. Creating "Smart" Surfaces Using Stimuli Responsive Polymers. *Adv. Mater.* **2002**, No. 17, 5.
(24) Chen, T.; Ferris, R.; Zhang, J.; Ducker, R.; Zauscher, S. Stimulus-Responsive Polymer Brushes on Surfaces: Transduction Mechanisms and Applications. *Progress in Polymer Science* **2010**, *35* (1–2), 94–112. https://doi.org/10.1016/j.progpolymsci.2009.11.004.
(25) Bhagawati, M.; Rubashkin, M. G.; Lee, J. P.; Ananthanarayanan, B.; Weaver, V. M.; Kumar, S. Site-Specific Modulation of Charge Controls the Structure and Stimulus Responsiveness of Intrinsically Disordered Peptide Brushes. *Langmuir* **2016**, *32* (23), 5990–5996. https://doi.org/10.1021/acs.langmuir.6b01099.
(26) Shenogina, N.; Godawat, R.; Keblinski, P.; Garde, S. How Wetting and Adhesion Affect Thermal Conductance of a Range of Hydrophobic to Hydrophilic Aqueous Interfaces. *Physical Review Letters* **2009**, *102* (15). https://doi.org/10.1103/PhysRevLett.102.156101.
(27) Banerjee, S.; Parimal, S.; Cramer, S. M. A Molecular Modeling Based Method to Predict Elution Behavior and Binding Patches of Proteins in Multimodal Chromatography. *Journal of Chromatography A* **2017**, *1511*, 45–58. https://doi.org/10.1016/j.chroma.2017.06.059.
(28) Godawat, R.; Jamadagni, S. N.; Garde, S. Characterizing Hydrophobicity of Interfaces by Using Cavity Formation, Solute Binding, and Water Correlations. *Proceedings of the National Academy of Sciences* **2009**, *106* (36), 15119–15124.
(29) Jamadagni, S. N.; Godawat, R.; Dordick, J. S.; Garde, S. How Interfaces Affect Hydrophobically Driven Polymer Folding †. *The Journal of Physical Chemistry B* **2009**, *113* (13), 4093–4101. https://doi.org/10.1021/jp806528m.
(30) Wang, J.; Wolf, R. M.; Caldwell, J. W.; Kollman, P. A.; Case, D. A. Development and Testing of a General Amber Force Field. *Journal of computational chemistry* **2004**, *25* (9), 1157–1174.

(31) Wang, J.; Cieplak, P.; Kollman, P. A. How Well Does a Restrained Electrostatic Potential (RESP) Model Perform in Calculating Conformational Energies of Organic and Biological Molecules? *Journal of computational chemistry* **2000**, *21* (12), 1049–1074.
(32) Bilodeau, C. L.; Lau, E. Y.; Cramer, S. M.; Garde, S. Conformational Equilibria of Multimodal Chromatography Ligands in Water and Bound to Protein Surfaces. *The Journal of Physical Chemistry* **2019**, *123* (23), 4833–4843.
(33) D.A. Case, R.M. Betz, D.S. Cerutti, T.E. Cheatham, III, T.A. Darden, R.E. Duke, T.J. Giese, H. Gohlke,; C., A. W. G., N. Homeyer, S. Izadi, P. Janowski, J. Kaus, A. Kovalenko, T. S. Lee, S. LeGrand, P. Li,; Lin, T. Luchko, R. Luo, B. Madej, D. Mermelstein, K.M. Merz, G. Monard, H. Nguyen, H.T. Nguyen, I.; Omelyan, A. Onufriev, D.R. Roe, A. Roitberg, C. Sagui, C.L. Simmerling, W.M. Botello-Smith, J. Swails,; R.C. Walker, J. Wang, R.M. Wolf, X. Wu, L. Xiao and P.A. Kollman. AMBER 2016. University of California, San Francisco 2016.
(34) Le Grand, S.; Götz, A. W.; Walker, R. C. SPFP: Speed without Compromise—A Mixed Precision Model for GPU Accelerated Molecular Dynamics Simulations. *Computer Physics Communications* **2013**, *184* (2), 374–380. https://doi.org/10.1016/j.cpc.2012.09.022.
(35) Salomon-Ferrer, R.; Götz, A. W.; Poole, D.; Le Grand, S.; Walker, R. C. Routine Microsecond Molecular Dynamics Simulations with AMBER on GPUs. 2. Explicit Solvent Particle Mesh Ewald. *J. Chem. Theory Comput.* **2013**, *9* (9), 3878–3888. https://doi.org/10.1021/ct400314y.
(36) Darden, T.; York, D.; Pedersen, L. Particle Mesh Ewald An N·log(N) Method for Ewald Sums in Large Systems. *The Journal of Chemical Physics* **1993**, *98* (10089), 10089–10092.
(37) Berendsen, H. J. C.; Postma, J. P. M.; van Gunsteren, W. F.; DiNola, A.; Haak, J. R. Molecular Dynamics with Coupling to an External Bath. *The Journal of Chemical Physics* **1984**, *81* (8), 3684–3690. https://doi.org/10.1063/1.448118.
(38) Huggins, D. J. Correlations in Liquid Water for the TIP3P-Ewald, TIP4P-2005, TIP5P-Ewald, and SWM4-NDP Models. *The Journal of Chemical Physics* **2012**, *136* (6), 064518. https://doi.org/10.1063/1.3683447.
(39) Karkov, H. S.; Krogh, B. O.; Woo, J.; Parimal, S.; Ahmadian, H.; Cramer, S. M. Investigation of Protein Selectivity in Multimodal Chromatography Using in Silico Designed Fab Fragment Variants. *Biotechnol. Bioeng.* **2015**, *112* (11), 2305–2315. https://doi.org/10.1002/bit.25642.
(40) Robinson, J.; Roush, D.; Cramer, S. Domain Contributions to Antibody Retention in Multimodal Chromatography Systems. *Journal of Chromatography A* **2018**. https://doi.org/10.1016/j.chroma.2018.05.058.
(41) Acharya, H.; Vembanur, S.; Jamadagni, S. N.; Garde, S. Mapping Hydrophobicity at the Nanoscale: Applications to Heterogeneous Surfaces and Proteins. *Faraday Discussions* **2010**, *146*, 353. https://doi.org/10.1039/b927019a.
(42) Xi, E.; Venkateshwaran, V.; Li, L.; Rego, N.; Patel, A. J.; Garde, S. Hydrophobicity of Proteins and Nanostructured Solutes Is Governed by Topographical and Chemical Context. *Proceedings of the National Academy of Sciences* **2017**, *114* (51), 13345–13350. https://doi.org/10.1073/pnas.1700092114.
(43) Parimal, S.; Garde, S.; Cramer, S. M. Interactions of Multimodal Ligands with Proteins: Insights into Selectivity Using Molecular Dynamics Simulations. *Langmuir* **2015**, *31* (27), 7512–7523. https://doi.org/10.1021/acs.langmuir.5b00236.